J Mater Sci (2010) 45:4358–4368
DOI 10.1007/s10853-010-4260-7

EUROMAT 2009

Influence of the brazing parameters on microstructure, residual stresses and shear strength of diamond–metal joints

Sebastian Buhl · Christian Leinenbach · Ralph Spolenak · Konrad Wegener

Received: 13 November 2009 / Accepted: 20 January 2010 / Published online: 6 February 2010

Abstract The reliability and integrity of diamond cutting tools depend on the properties of diamond–metal joints as created by a brazing process. Block-shaped monocrystalline diamonds were brazed onto a steel substrate (X2CrNiMo 18-14-3), using silver–copper based Cusil-ABA^{TM} (Ag–35wt%Cu–1.75wt%Ti) filler alloy. The experimental procedure includes a thorough microstructural investigation of the filler alloy, the determination of the induced residual stresses by Raman spectroscopy as well as the joint's shear strength utilizing a special shear device. The brazing processes were carried out at 850, 880 and 910 °C for dwell durations of 10 and 30 min, respectively. At the steel interface two interlayers develop. The layers grow with extended dwell duration and higher brazing temperature. The residual stresses only slightly depend on the brazing parameters and exhibit a maximum value of −400 MPa. Unlike the residual stresses, the shear strength strongly depends on the brazing parameters and thus on the microstructure. Three failure modes could be identified; a ductile fracture in the filler alloy, a brittle fracture in the interlayers and a partly shattering of the diamond.

S. Buhl (✉) · K. Wegener
Institute of Machine Tools and Manufacturing, ETH Zurich, Tannenstrasse 3, 8092 Zurich, Switzerland
e-mail: buhl@iwf.mavt.ethz.ch

S. Buhl · C. Leinenbach
Laboratory for Joining and Interface Technology, EMPA Duebendorf, Ueberlandstrasse 129, 8600 Duebendorf, Switzerland

R. Spolenak
Laboratory for Nanometallurgy, ETH Zurich, Wolfgang-Pauli-Strasse 10, 8093 Zurich, Switzerland

Introduction

The application of diamond as an abrasive component in material removal tools, e.g. for grinding and cutting, is evident due to its outstanding hardness, high strength and high wear resistivity, directly linked to its covalent structure. Different ways exist to attach diamond onto a substrate; either mechanical bonding between diamond and substrate, i.e. resin-bonding, sintering or electroplating, or chemical bonding, i.e. active brazing with Cu-, Ni,- or Ag-based filler alloys. Brazed single-layer diamond grinding tools possess several benefits in comparison to electroplated ones. Owing to the chemical bond the diamond grain is more firmly fixed to the tool body. The high bond strength leads to a larger grain protrusion and this in turn results in more space for coolant flow, which improves the cooling and/or for storage of the chips. It signifies an increase in tool service life and process cutting speed [1–4]. However, there are some disadvantages of brazed diamonds. From extensive cutting experiments with brazed diamond tools performed by the present authors, different kinds of grain failure could be detected, namely grain fracture, interface fracture between the diamond and the filler alloy, abrasion of the bond by chip flow, abrasion of the grain and maybe even fatigue, which may cause catastrophic damage in sparsely grained abrasive layers. This indicates that failure of brazed diamond components is a complex mechanism that involves the brazing process, the specific properties of diamond grains, the filler alloy and the interlayers developed during the manufacturing process as well as the residual stresses arising from the mismatch in the thermal expansion coefficients during the brazing process.

Previous investigations revealed the formation of a titanium-carbide (TiC) layer at the diamond interface,

whose thickness depends on the brazing conditions [5, 6]. The effect of this TiC layer on the residual stresses and the mechanical properties of the joint is still unclear. It is known that the filler alloy microstructure has a significant influence on the mechanical properties of metal–ceramic joints [7]. Due to the non-equilibrium conditions the formation of brittle phases in the filler alloy as well as at the interfaces can occur, which is possibly related to the interfacial strength.

No precise data are available in literature on the influence of the brazing parameters on the microstructure, on the formation of residual stresses in brazed diamonds as well as on quantitative measurements of diamond–metal joints' shear strengths.

Considering residual stresses Raman spectroscopy has proved successful in terms of quantifying stresses in microelectronics [8] and in chemical vapor deposition (CVD) diamond films [9, 10]. Stresses in Raman-active materials are indicated by a shift in the wavenumber of the so-called Raman–Stokes-peak in the Raman-spectrum compared to that of a stress-free specimen. A lot of scientific research was spent to quantify the peak shift for diamond in dependence of the externally applied stress [11–22]. A linear relationship was found for the case of a hydrostatic stress state. Raman measurements can be performed very fast and due to the high resolution the investigated material volume is very small. For this reason the residual stresses can be determined very locally at the interesting sites of a specimen, e.g. in the vicinity of interfaces and at edges.

Only little information on the mechanical performance of brazed diamonds can be found in the literature. An overall aim is to have the possibility to calculate the retention force for each single grain in a stochastic model from its interface geometry. Klocke et al. [23] developed a grain pullout system. Single brazed diamond grains were loaded with a special device and the force at which failure occurred is determined. The drawback of this method is the unknown interfacial area between the diamond and the filler alloy, which makes an exact quantitative measurement impossible. The shear strength of a brazed CVD diamond on a hard metal substrate was investigated in Ref. [24]. The failure in the joint was induced by an increasing force and the shear strength is calculated from the maximum force and the apparent contact area. Another shear test device was developed by Siegmann et al. [25], mainly for testing the bond strength of ceramic coatings on metals. The load on the specimen can be introduced parallel and next to the interface. It yields to informative and quantitative results combined with easy specimen geometry, quick preparation and testing.

The scope of this work is to identify possible correlations between the microstructure, the residual stresses and the shear strength of brazed diamond–metal joints using a silver-based filler alloy. In order to investigate the influences of the brazing parameters, the specimens were brazed at three different temperatures for two dwell durations.

Experimental

Materials and brazing process

The test specimens used for this work consist of three parts: a steel substrate, the active braze alloy and a block-shaped monocrystalline diamond (cf. Fig. 1). The substrate material was an austenitic stainless Cr–Ni–Mo steel (X2CrNiMo 18-14-3) plate with the geometry 30 × 10 × 5 mm. Its dimensions were adapted to the specimen's holder of the shear device, which is described below. As active filler alloy Cusil-ABA^{TM} (−325 mesh; Ag–35wt%Cu–1.75wt%Ti) from Wesgo Metals (Hayward, CA, USA) with titanium as reactive element was used. According to Ref. [26] the solidus temperature is 780 °C and the liquidus temperature is 815 °C. The diamonds were block-shaped monocrystalline diamonds (MT L 101005Q^{TM}, Element Six e6, Isle of Man, UK) with dimensions 1.0 × 1.0 × 0.5 mm. The diamond is oriented on the (100) cubic plane [27]. Additionally, one of the lateral surfaces was carefully polished. Block-shaped diamonds were used because they exhibit a well-defined geometry of the interface compared to standard diamond grains and therefore are adequate for the desired investigations. The mechanical properties of the substrate as well as of the filler alloy and the diamond are listed in Table 1 [26, 28–30].

Prior to the brazing process the substrates were ultrasonically cleaned with acetone and subsequently degassed at a base pressure of $p = 10^{-5}$–10^{-6} mbar for 45 min at 800 °C in a Torvac high-vacuum furnace (Cambridge

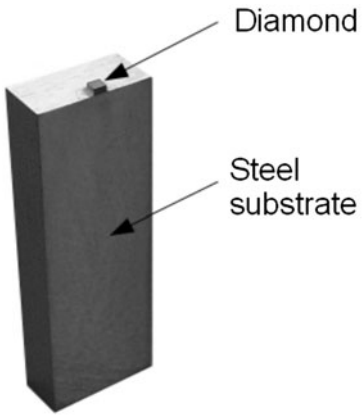

Fig. 1 Applied specimen design; an austenitic stainless steel substrate (X2CrNiMo 18-14-3) and a block-shaped monocrystalline diamond (Monodite MT L 101005Q^{TM}), brazed with Cusil-ABA^{TM}

Table 1 Mechanical properties of the used materials

Material	Young's modulus (GPa)	Yield strength (MPa)	Tensile strength (MPa)
St 1.4435	200	200	500–700
Cusil-ABA	83	271	346
Diamond	1050	–	7500–12500[a]

[a] Compressive fracture strength on (111) surface [26, 28–30]

Vacuum Engineering LTD, Cambridge, UK) in order to remove organic residues in the surficial layers of the substrate due to machining. Afterwards, the filler alloy was applied as a paste. An almost identical thickness after drying at 150 °C of (122 ± 4) µm was achieved for all specimens. The diamond was then placed on the filler alloy with the polished lateral surface at the edge of the substrate, as can be seen in Fig. 1. This design was chosen to allow all necessary investigations in a thorough way at the same specimen.

Brazing was carried out in the above mentioned high vacuum furnace ($p = 10^{-5}$–10^{-6} mbar) at 850, 880 and 910 °C for 10 and 30 min, respectively, using a special brazing jig. Five specimens were brazed for the two batches at 880 °C and three specimens each in the cases of 850 and 910 °C, respectively. Loading the joint with a small weight (~2 g) prevented floating and rotating of the diamond during brazing and ensured sufficient wetting. After cooling in the high vacuum furnace (cooling rate: 20 K/min), the specimens were ground and polished using diamond containing suspensions down to a grain size of 1 µm. The scope of the grinding and polishing processes was the removal of the surplus filler alloy at the lateral side of the specimen for obtaining a metallographic section (steel–filler alloy–diamond).

Characterization methods

A thorough microstructural investigation of the filler alloy was carried out using a Hitachi S-4800 high-resolution scanning electron microscope (SEM, Hitachi-High Technologies, Tokyo, Japan). The atomic composition of the observed phases and layers was identified by means of energy dispersive X-ray spectroscopy (EDX, INCAPentaFETx3, Oxford Instruments, High Wycombe, UK).

Raman spectroscopy was applied as a fast method for measuring the residual stresses. A WITec Confocal Raman Microscope 200 (WITec, Ulm, Germany) with a laser as light source (wavelength: 442 nm; Omnichrome Series 74, Melles Griot Laser Group, Carlsbad, CA, USA) was used. The microscope exhibits a lateral resolution of 300 nm and a vertical resolution of 600 nm. All measurements were run at ambient temperature. The residual stresses were determined via the shift in the wavenumber ω of the diamond Raman–Stokes-peak, compared to the wavenumber ω_0 of the stress-free diamond. The wavenumber of the Raman–Stokes-peak for an unstressed diamond at room temperature is $\omega_0 \approx 1332\ \mathrm{cm}^{-1}$.

With regard to the literature [11–22], the hydrostatic stress $\sigma_{\mathrm{hydrostatic}}$ in a diamond can be calculated according to Eq. 1:

$$\sigma_{\mathrm{hydrostatic}} = A_{\mathrm{hydrostatic}} \cdot (\omega - \omega_0) = A_{\mathrm{hydrostatic}} \cdot \Delta\omega \qquad (1)$$

where $A_{\mathrm{hydrostatic}}$ denotes the so-called hydrostatic pressure coefficient and $\Delta\omega$ is the shift in the wavenumber of the diamond's Raman–Stokes-peak.

Taking not only experimental determination of the hydrostatic pressure coefficient into account [11–19], but also atomistic simulations [20–22], the mean value and the standard deviation of the hydrostatic pressure coefficient is $A_{\mathrm{hydrostatic}} = (-0.347 \pm 0.017)\ \mathrm{GPa/cm}^{-1}$. According to Occelli et al. [19], the peak shift–stress relationship can be described by a quadratic fit. However, the quadratic term only influences the peak shift significantly at pressures higher than 20 GPa. Since such high stresses did not occur in our measurements, the quadratic term can be neglected. The error in the calculated hydrostatic stress, if neglecting the quadratic term for low stresses (max. −400 MPa), is less than 0.1%.

For a biaxial stress state the proportionality factor A_{biaxial} can be determined using the secular equation of Ganesan et al. [31], the approximation of Anastassakis et al. for small strains [32] and the general Hooke's law; analogous to [33]. Due to the back-scattering setup of the Raman microscope, the fact that the biaxial stress state is parallel to the penetrating laser, the arrangement between the laser and the diamond lattice as well as $\sigma_{11} = 0$ MPa and $\sigma_{22} = \sigma_{33} = \sigma_{\mathrm{biaxial}}$ the biaxial stress $\sigma_{\mathrm{biaxial}}$ can be calculated with Eq. 2

$$\sigma_{\mathrm{biaxial}} = A_{\mathrm{biaxial}} \cdot (\omega - \omega_0) = A_{\mathrm{biaxial}} \cdot \Delta\omega \qquad (2)$$

with

$$\begin{aligned} A_{\mathrm{biaxial}} &= 2 \cdot \omega_0 / [p \cdot (S_{11} + S_{12}) + q \cdot (S_{11} + 3 \cdot S_{12})] \\ &= -0.43\ \mathrm{GPa/cm}^{-1} \end{aligned} \qquad (3)$$

where $S_{11} = 1.01\ \mathrm{TPa}^{-1}$, $S_{12} = -0.14\ \mathrm{TPa}^{-1}$ and $S_{44} = 1.83\ \mathrm{TPa}^{-1}$ are the elastic compliance constants of diamond [34] and p, q, r denote the diamond's phonon deformation potentials with the values $p = -2.82 \cdot \omega_0^2$, $q = -1.78 \cdot \omega_0^2$ and $r = -1.89 \cdot \omega_0^2$ according to Ref. [35].

For the stress analysis, the wavenumber of the first measurement point for every test point was set as wavenumber ω_0. This decision was made based on the assumption that the lateral surface of the diamond after brazing is stress-free due to the specimen's design. The

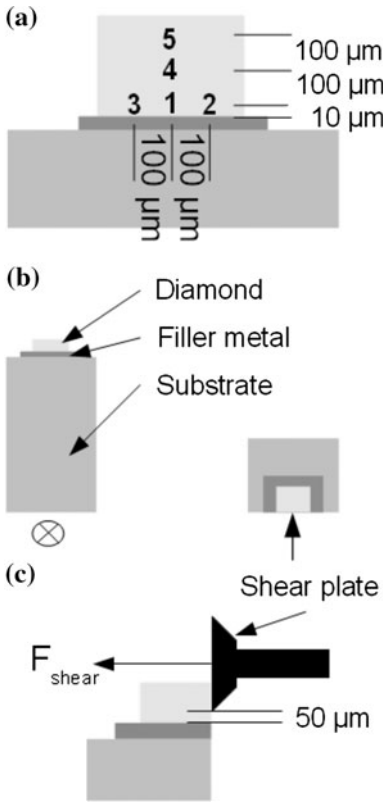

Fig. 2 The sketches show the numeration and the sites of the test points (**a**), the description of the parameter depth (**b**) and a schematic of the shear test (**c**)

obtained results are displayed as stress–depth graphs, calculated either with Eq. 1 or 2 and averaged over 10 data points. Figure 2a shows a sketch of the specimen with the various test points for the residual stress measurements. The test point No. 1 is situated in the middle of the diamond's lateral surface approximately 10 µm above the interface. The test points No. 2 and No. 3, also 10 µm above the interface, are shifted 100 µm to the right and to the left, respectively. The test points with the distances of 110 and 210 µm from the filler alloy–diamond interface are denoted with No. 4 and No. 5. The direction of measurement, which is perpendicular to the polished lateral surface of the specimen and parallel to the filler alloy–diamond interface, is described by the parameter "depth" (cf. Fig. 2b). A Raman-spectrum was recorded every 0.8 µm and the wavenumber of the Raman–Stokes-peak was analyzed. The analysis was made with the program WITec Project 1.92 (WITec, Ulm, Germany). The maximum depth for a satisfactory Raman signal is ~250 µm.

The joint's shear strength was determined using a STM-20 A shear testing device (Walter + Bai AG Testing Machines, Loehningen, Switzerland), allowing a maximum force of 4 kN. The precise description of the device has been described elsewhere [25]. Due to the special design of the shear tester, the load on the specimen is introduced parallel at a distance of approximately 50 µm from the filler alloy–diamond interface (cf. Fig. 2c). The tests were run under displacement control with a shear rate of 0.1 mm/s until failure of the joints occurred. During the experiments load–displacement diagrams were recorded and the maximum load was converted into the shear strength by dividing it by the brazed diamond surface area ($A_{\text{brazed diamond}} = 1\ \text{mm}^2$). The tests were performed under ambient temperature.

Results

Microstructural investigation

The SEM micrograph in Fig. 3 presents an overview of the complete brazing gap for a sample brazed at 850 °C for 10 min. Figure 4 shows representative micrographs of the filler alloy–steel interface for the specimens brazed at 880 °C for 10 min (a) and 30 min (b). Four different phases are visible, i.e. two layers (L1 and L2) directly on top of the steel substrate and two solid solution phases arising from the eutectic solidification. In addition to that, it is known from previous investigations that a TiC layer at the diamond interface forms, whose thickness depends on the brazing conditions [5, 6]. However, this layer is rather thin (~50–100 nm) and cannot be seen in the micrographs. From Fig. 4b it can be seen that primary-(Cu) has precipitated additionally as larger grains. The interface between the steel and the interlayer L1 is not always clearly visible, making the determination of the thickness difficult. The interlayer L2 possesses a clearly visible undulating interface towards the eutectic region, whereas it is straight between the two interlayers. It was found that the

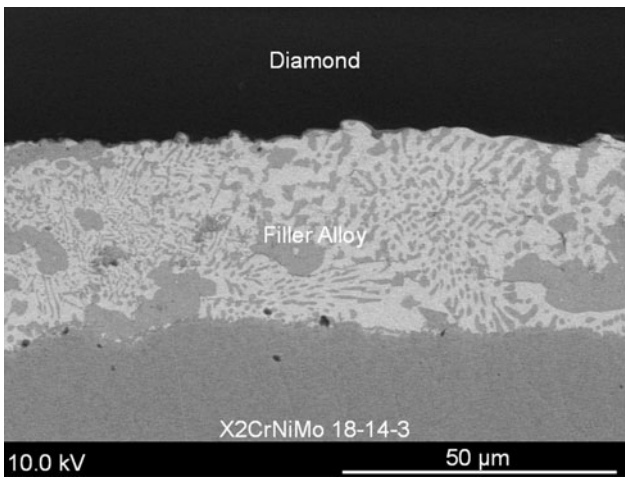

Fig. 3 The SEM micrograph shows the complete brazing gap of a sample brazed at 850 °C/10 min

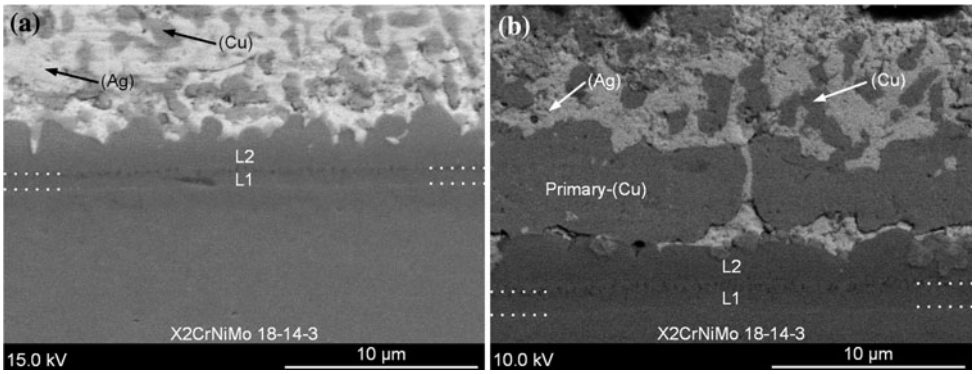

Fig. 4 The SEM micrographs show the filler alloy–steel interface of the samples brazed at 880 °C for 10 min (**a**) and 30 min (**b**). The interlayers L1/L2 can be seen as well as the eutectic region with the copper-rich (Cu) and silver-rich (Ag) solid solution. In micrograph (**b**) primary-(Cu) has precipitated in addition

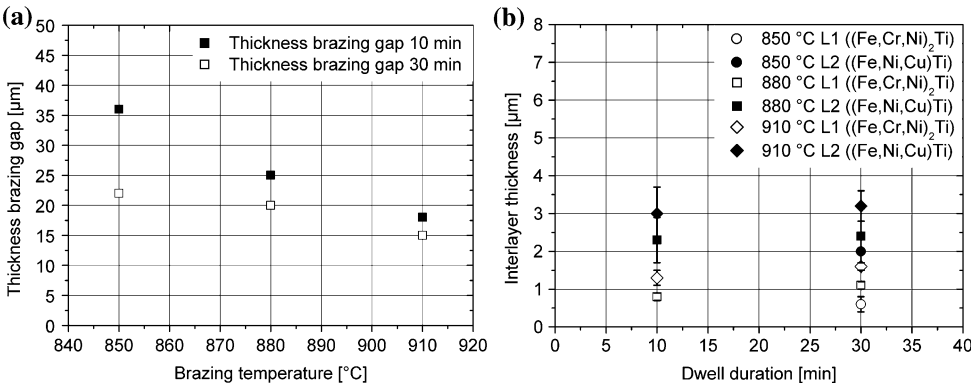

Fig. 5 The effect of the brazing temperature and the dwell duration on the thicknesses of the brazing gap (**a**) and on the growth of the two interlayers L1 and L2 (**b**)

thicknesses of the brazing zone as well as the thicknesses of the interlayers L1 and L2 strongly depend on the brazing parameters.

Although the initial filler alloy thickness was identical for every batch, the final thickness of the brazing gap depends on the brazing parameters, as can be seen in Figs. 3 and 5a. The thicknesses of the brazing gaps decrease with increased brazing temperature and extended dwell duration. The final brazing gap thickness of the samples brazed at 850 °C/10 min is 36 µm, which decreases to 15 µm for 910 °C/30 min. This is presumably due to the higher spreading ability of the molten filler alloy which is affected by the higher temperature, making the molten filler alloy more fluid for longer dwell durations. The thicknesses of the interlayers L1 and L2 as functions of the brazing time and dwell durations are shown in Fig. 5b. For a brazing temperature of 850 °C and a dwell duration of 10 min, the two interlayers could not be clearly resolved. It could be stated that the intermetallic layer L1 grows with higher brazing temperature and extended holding time, whereas for the interlayer L2 only a tendency to grow can be assumed. The interlayer L2 is always thicker than the interlayer L1. Comparing the interlayer thicknesses in the temperature range between 850 and 910 °C at a dwell duration of 30 min, it highlights that the thickness of the interlayer L1 at 910 °C is approximately three times that of 850 °C, although it increases only by about 50% in case of the interlayer L2. The interfacial layer next to the steel substrate (L1) has large amounts of iron (40.6–48.5 at.%) and titanium (28.9–43.1 at.%). The amounts of chromium and nickel in this phase are 10.0–16.5 at.% and 3.0–4.5 at.%, respectively, depending on the brazing temperature and the dwell duration. The overlaying intermetallic layer L2 consists of 24.2–44.6 at.% Fe and 32.8–47.3 at.% Ti, besides the incorporation of nickel vary between 9.8 and 18.0 at.%, whereas the amount of copper is in the range between 4.9 and 17.0 at.%. Also, traces of chromium and silver are detected. Although EDX measurements do not allow a clear identification of the phases, it is concluded from the compositions that the interlayer L1 is $(Fe,Cr,Ni)_2Ti$ and that the interlayer L2 is (Fe,Ni,Cu)Ti. The solid solution phases in the eutectic region are a copper-rich one, labelled (Cu) and a silver-rich one, labelled (Ag). The (Cu)-phase exhibits approximately 96.0 at.% Cu, whereas the (Ag)-phase contains between 85.1 and 92.7 at.% silver and some titanium.

Residual stresses

In Fig. 6a, a comparison between the Raman–Stokes-peak of an unbrazed diamond ($\omega_0 = 1332.2\ cm^{-1}$) as well as of a brazed diamond ($\omega = 1333.2\ cm^{-1}$) is shown; the shift in the wavenumber of the Raman–Stokes-peak of the brazed diamond can be clearly seen. The shift in the

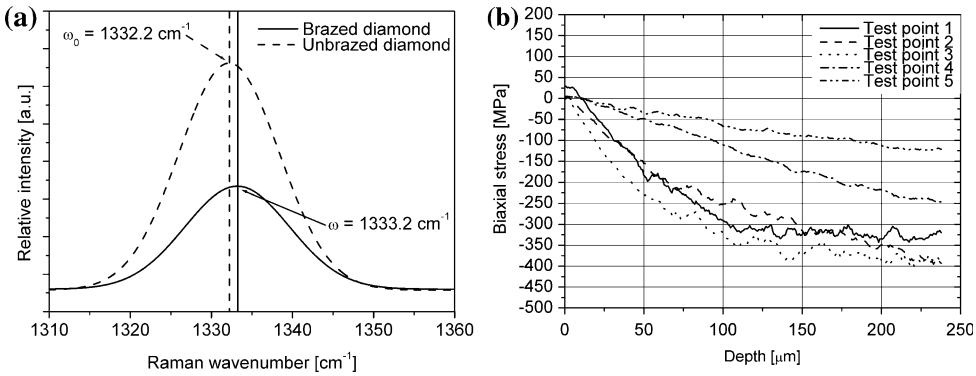

Fig. 6 The diagram (**a**) shows the shift in the wavenumber of the Raman–Stokes-peak of a brazed diamond compared to an unbrazed one. The graph (**b**) displays the depth-dependence of the residual stresses for the brazing parameters 850 °C and 10 min. The data of the residual stresses were calculated using Eqs. 2 and 3 and then presented as a 10-data point moving average

wavenumber and a possible split of the Raman–Stokes-peak represent the sum of the acting stresses [36], more precisely the weighted average of the stress tensor components [37]. A shift to a higher wavenumber ω of the Raman–Stokes-peak compared to ω_0 indicates compressive stresses in the diamond, whereas tensile stresses are characterized by a shift to values ω lower than ω_0. From a mechanical consideration the diamond is not constrained at its top surface, it can freely expand due to the geometry of the sample. Consequently, a biaxial stress state is much more likely than a hydrostatic one. In order to calculate the biaxial stress, Eqs. 2 and 3 are used. The accuracy of the biaxial residual stresses determined with error propagation is ±10 MPa.

The measured residual stresses are shown in Figs. 6b and 7. Figure 6b shows the stress–depth graphs at the five test points for a joint brazed at 850 °C for 10 min. A linear increase of the compressive residual stresses from the lateral surface of the diamond to the maximum depth can be observed. Near the interface, at the test points No. 1 to No. 3, a stress plateau occurs at depths larger than 150 μm. For the test points No. 4 and No. 5 this plateau was not observed, but it cannot be excluded that this stress plateau will occur at higher depths, where the measurements cannot be performed due to the strong weakening of the Raman signal. The maximum residual stresses near the interface are between −325 MPa and −400 MPa. An increasing distance to the interface (test points No. 4 and

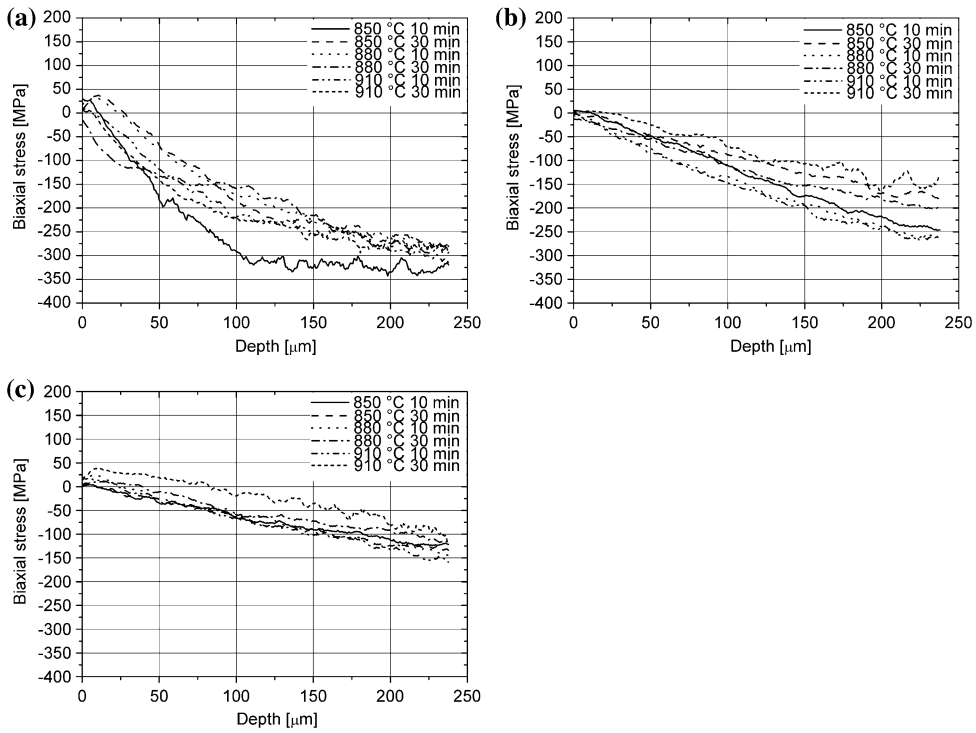

Fig. 7 The influence of the brazing parameters on the development of the residual stresses at the test points No. 1 (**a**), No. 4 (**b**) and No. 5 (**c**). Altering the brazing parameters result in insignificant variations of the residual stress–depth graphs

No. 5) leads to lower acting compressive residual stresses. The maximum residual stress at a distance of 110 μm (test point No. 4) above the interface is −250 MPa and at a distance of 210 μm (test point No. 5) it is approximately −125 MPa. Rather similar observations were made for the specimens brazed with other brazing parameters, as can be seen in Fig. 7. For some specimens, slight tensile stresses were measured close to the interface at the specimen surface, which are interpreted as disturbances from the surface. Furthermore, taking the calculated stress error into account, it can be assumed that the residual stress values for the different specimens are very similar. For this reason it can be concluded that the residual stresses only slightly depend on the brazing parameters. Due to a lack in statistics, it is assumed that there is a tendency to lower residual stresses, when increasing the brazing temperature and the dwell duration. This might be explained by the longer cooling process for higher brazing temperatures, resulting in more time for stress relaxation during cooling. This means that the possibility for stress relaxation is enhanced when brazing is carried out at higher temperatures. The comparison reveals that the stress decreases by 17% within the first 100 μm for specimens brazed for 10 min and by 42% for specimens brazed for 30 min. The decay within a distance of 200 μm is 58% for both holding times.

Shear strength and fracture behavior

Table 2 displays the values of the shear strength for the different brazing parameters. For a brazing temperature of 850 °C the shear strength values differ significantly between the single specimens. Nevertheless, it can be stated that the shear strengths are very similar, thus it is assumed that the longer dwell duration did not affect significantly the shear strength. The maximum values are (389 ± 8) MPa for 10 min and (364 ± 7) MPa for 30 min holding time. It seems that at a brazing temperature of 880 °C the extended dwell duration results in higher values by about 40 MPa. The opposite is observed at 910 °C, where the maximum shear strength value drops off from (392 ± 8) MPa to (220 ± 4) MPa.

During the shear process three failure "modes" were observed. First, the samples fail due to fracture in the filler alloy (Fig. 8a, b). Secondly, a partly shattering of the diamond occurred on some specimens (Fig. 8c, d) and last a brittle fracture in the interlayers L1/L2 (Fig. 8e, f). These three "modes" often appear simultaneously on one sample. In Fig. 8a and b (850 °C, 30 min, specimen 3), ductile fracture occurs in the filler alloy, which results in a high shear strength of (364 ± 7) MPa. This is due to the plasticity and hardening of the filler alloy. A shear process going along with the shattering of the diamond leads to significant smaller values of the shear strength; the upper limit of the shear strength in this case is approximately 200 MPa. The partial destruction of the diamond might be the result of a not fully parallel orientation of the shear plate relatively to the diamond during testing, leading to pronounced stress maxima at the contact point between the shear plate and the diamond. In Fig. 8c and d, the specimen No. 5 brazed at 880 °C for 30 min displays this situation. The sample No. 1 brazed at 910 °C for 30 min shows a fracture path which mainly proceeds through the interlayers (see Fig. 8e, f) and exhibits a shear strength value of (220 ± 4) MPa.

Table 2 Shear strength values for the different brazing parameters

Brazing parameters	Sample no.	Shear strength (MPa)	Diamond shattered
850 °C, 10 min	1	201 ± 4	X
	2	154 ± 3	–
	3	389 ± 8	–
850 °C, 30 min	1	178 ± 4	X
	2	238 ± 5	X
	3	364 ± 7	–
880 °C, 10 min	1	165 ± 3	X
	2	119 ± 3	X
	3	233 ± 5	–
	4	160 ± 3	X
	5	161 ± 3	–
880 °C, 30 min	1	201 ± 4	–
	2	239 ± 5	–
	3	198 ± 4	–
	4	–	–
	5	212 ± 4	X
910 °C, 10 min	1	318 ± 6	–
	2	392 ± 8	–
	3	226 ± 5	X
910 °C, 30 min	1	220 ± 4	–
	2	–	–
	3	124 ± 3	X

Discussion

Microstructural investigation

The formation of different interlayers is often found when brazing metal–ceramic joints with an active silver–copper based filler alloy and titanium as the reactive element [7, 38, 39]. Here, two interlayers, namely $(Fe,Cr,Ni)_2Ti$ and (Fe,Ni,Cu)Ti, on top of the steel substrate are formed, whose thicknesses are influenced by the brazing parameters. They grow with increased brazing temperature and

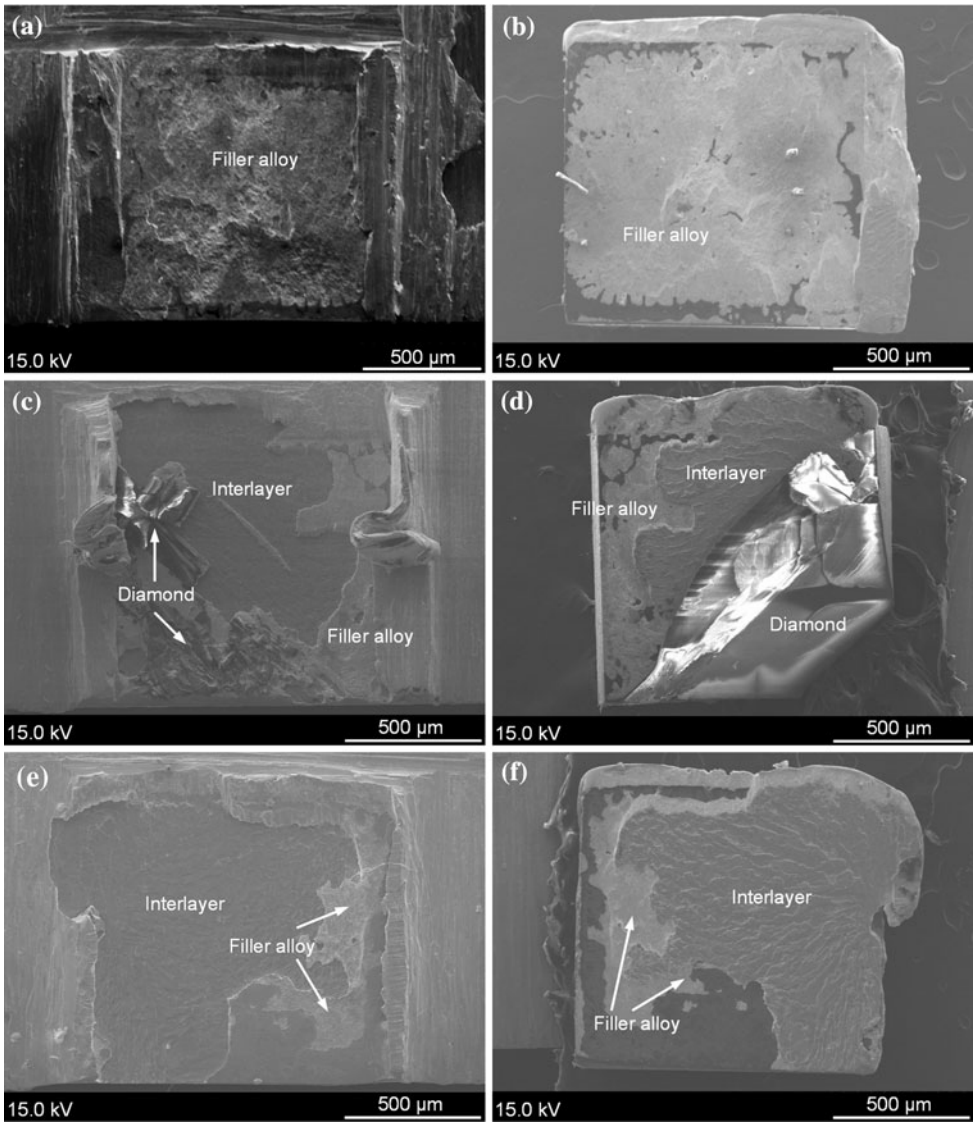

Fig. 8 The micrographs (**a**–**f**) show the shear surfaces; (**a**), (**c**) and (**e**) on the steel substrate and (**b**), (**d**) and (**f**) those on the diamond side for samples brazed at 850 °C for 30 min (**a**) and (**b**), at 880 °C for 30 min (**c**) and (**d**) and at 910 °C for 30 min (**e**) and (**f**)

longer holding time, whereas the total thickness of the brazing gap decreases. This indicates that the percentage of brittle interlayers at the brazing gap relative to the total thickness increases, which may influence the residual stresses and the shear strength as it is discussed below. The eutectic region of the solidified filler alloy contains (Cu) and (Ag) solid solutions. The copper content of the (Cu) solid solution with approximately 96 at.% agrees well with literature data [40], like the composition of the (Ag) solid solution [38] with approximately 90 at.% silver.

Residual stresses

The Raman-spectra clearly show the development of compressive residual stresses in the diamond after brazing. The scattering of the results as shown in Fig. 6b at the interface and in Fig. 7a–c can be a result of a locally inhomogeneous wetting of the diamond, a locally different reaction layer thickness, the fact that the interface is not completely even or of impurities in the diamond.

The residual stresses in the diamond might arise from the mismatch in the thermal expansion coefficient of metal (filler alloy, steel) and diamond and/or from a lattice mismatch between the diamond and the adjacent phase in the solidified filler alloy, i.e. a TiC layer. Klotz et al. showed with TEM investigations that stacking faults in brazed diamonds with a (111) orientation are created directly at the interface to the TiC layer, which also has a (111) orientation. They assumed that residual stresses in the GPa range are responsible for these stacking faults [5, 6]. This assumption would be supported by the large misfit of the inter-planar spacing of the (111) planes between diamond (0.206 nm) and TiC (0.2499 nm).

Thermal residual stresses σ_{th} in the diamond arising from the different thermal expansion coefficients between diamond and filler alloy can be calculated according to Eq. 4

$$\sigma_{th} = E \cdot \Delta\alpha \cdot \Delta T \quad (4)$$

where E is the Young's modulus, $\Delta\alpha$ denotes the mismatch in the thermal expansion coefficients between diamond and Cusil-ABA^{TM} and ΔT is the temperature difference between the brazing temperature and room temperature.

Using the corresponding values for diamond and filler alloy and assuming a brazing temperature of 880 °C ($E_{diamond} = 1050$ GPa [29], $\Delta\alpha = -17.4 \times 10^{-6}$ K^{-1} [26, 41], $\Delta T = 860$ K), thermal residual stresses as high as −15.7 GPa would be expected in the diamond.

However, compressive residual stresses of maximum −400 MPa were measured at a distance of 10 µm above the interface between the diamond and the filler alloy. This means that pronounced stress relaxation must have occurred. The most likely relaxation process is the plastic deformation of the filler alloy during cooling, due to its low yield strength [41, 42] compared to the diamond. The formation of the TiC layer at the filler alloy–diamond interface could also contribute to the relief of residual stresses due to an elastic deformation of the TiC layer [41]. The linear expansion coefficient of TiC (7×10^{-6} K^{-1} [43]) is in-between those of diamond (1.1×10^{-6} K^{-1} [41]) and Cusil-ABA (18.5×10^{-6} K^{-1} [26]). The influence of the microstructure on the residual stresses is low. It seems that the increasing thickness of the TiC layer [5, 6] with increasing brazing temperature has only a small effect on the development of residual stresses. In order to obtain force equilibrium, the compressive residual stresses in the diamond have to be compensated by tensile stresses in the filler alloy. The maximum residual stress at the interface inside the diamond is in the range of the filler alloy's yield strength (271 MPa) and tensile strength (346 MPa) at room temperature (cf. Table 1). This means that the stresses are relieved by plastic deformation of the filler alloy during cooling.

Residual stresses in the range of GPa appeared in diamond films deposited via CVD on various metallic substrates [36, 41, 44, 45]. In these cases, both the Raman–Stokes-peak shifts strongly and the peak is split up, leading to large biaxial residual stresses in the range of −3 GPa to −12 GPa. However, CVD diamond films normally exhibit various defects compared to a well-grown diamond depending on the deposition conditions, which also influence the residual stresses. Furthermore, the CVD films are directly deposited onto to a substrate without any ductile or stress-relieving interlayer. Kohzaki et al. [46] brazed a diamond film on top of a steel substrate, using an Ag–Cu–In–Ti filler alloy. The estimated compressive residual stress after brazing is determined via the shift in the wavenumber of the Raman–Stokes peak and is about −8 GPa. According to Ref. [46] this is due to the mismatch in the thermal expansion coefficients. The final conclusion is that the thermal residual stresses in brazed diamonds only slightly depend on the brazing parameters with the exception of the yield strength of the filler alloy. Compared to the diamond's strength of several GPa (cf. Table 1), the residual stresses are very low on average.

Shear strength and fracture behavior

In contrast to the residual stresses, the shear strength obviously strongly depends on the brazing parameters and thus on the microstructure of the joint, i.e. the interfacial layers as well as the total filler alloy thickness. The influence of residual stresses on the shear strength can be almost neglected, due to the fact that all specimens exhibit rather similar values. An increase of the brazing temperature as well as of the dwell duration leads to a decrease in filler alloy thickness and an increase of the interlayer thickness. This means that the percentage of brittle intermetallics with respect to the total filler alloy thickness increases. The excessive formation of intermetallic phases with higher brazing temperature, decreasing the shear strength, is reported in Ref. [47]. An influence of the microstructure on the mechanical performance could also be found for steel–alumina joints brazed with Ag–Cu–Ti filler alloy [7]. Compared to the reported shear strength of 130 MPa of a 110 µm thick CVD diamond film brazed (Ag–Cu–Ti filler alloy) on a hard metal substrate [48], our results are quite high. This can be explained by the differences in the mechanical properties of the filler alloy as well as in the structure and the dimensions of the diamond and the CVD diamond film.

The influence of the microstructure on the fracture behavior in our experiments, demonstrated by means of the shear surfaces, can be seen in Fig. 8a–f. At a brazing temperature of 850 °C, the interlayers are relatively thin and the thickness of the brazing gap is comparably large. This promotes a ductile fracture in the filler alloy, resulting in high shear strength values. At 880 °C for 10 min, the joint's failure directly occurred at the filler alloy–steel interface, resulting in low shear strengths, whereas at 30 min the fracture path partly proceed in the filler alloy and the interlayers (see Fig. 8c, d). The fracture path through the brittle interlayers is responsible for the decrease of the shear strength compared to the brazing temperature of 850 °C. The interlayers' microstructure is polycrystalline and exhibits microstructural defects like pores, etc. Compared to the ductile filler alloy the brittle interlayers are more susceptible to microstructural defects, due to their disability to deform plastically. At the present

defects a stress concentration is likely, which reduces the overall interlayer strength. Now, the application of an external load will exceed the critical fracture strength faster for the interlayers than for the filler alloy and an unstable crack propagation will take place. At 910 °C for 30 min holding time, the fracture almost completely proceeds in the interlayers. Therefore, the weakest links are now the thick intermetallic layers. The shear strength value is in the range of those brazed at 880 °C for 30 min. The shear strength values for a brazing temperature of 910 °C and 10 min holding time are in the range of those obtained at 850 °C. The difference to 10 min holding time is that the fracture path partly goes through the filler alloy and the interlayers. It appears that with increasing brazing temperature and holding time the fracture, associated with a higher percentage of brittle intermetallics in the brazing gap, is shifted from the ductile filler alloy to the brittle interlayers, which results in a decrease of the shear strength. Furthermore, it should be mentioned that no fracture in the TiC interlayer was observed, despite its inherent brittleness. Due to the thinness of the interlayers, the crack propagation does not proceed in the TiC interlayer, it will immediately shift into the filler alloy. This can be seen in Fig. 8c, where next to the shattered diamond pieces the filler alloy microstructure is observed and not the TiC microstructure. It seems that the interfacial strengths between TiC and diamond as well as TiC and filler alloy are high compared to the strengths of the filler alloy and the interlayers L1/L2 as well. This fact is confirmed by Fig. 8a, b, e and f where the cracks always run in the filler alloy or in the interlayers and not at the TiC–diamond interface. A concept for obtaining high shear strength of the joints might be brazing at temperatures slightly above the liquidus temperature. This results in a thin interlayer at the filler alloy–steel interface as well as a wide brazing gap. These two facts promote ductile fractures in the filler alloy and therefore high shear strengths of the joint. The influence of the holding time on the joint's shear strength at low brazing temperatures is rather negligible. However, due to the small number of tested joints, only a tendency for an increase in shear strength can be given.

Summary and conclusions

The influence of the brazing parameters, i.e. brazing temperature and dwell duration, on the properties of diamond–metal joints was investigated. The active filler alloy Cusil-ABA^{TM} provided sufficient bonding of the materials. The application of block-shaped monocrystalline diamond ensured a defined interface towards the filler alloy. The investigated characteristics are the microstructure, the development of thermal residual stresses and the joints' shear strengths. The microstructural investigations revealed two interlayers, namely $(Fe,Cr,Ni)_2Ti$ and (Fe,Ni,Cu)Ti, at the filler alloy–steel interface in addition to the well-known TiC layer at the filler alloy–diamond interface. The interlayers' thicknesses increased with brazing temperature and holding time, whereas the total thickness of the brazing gap decreases. This leads to a higher percentage of brittle interlayers at the total brazing gap, influencing the shear strength. Our investigations revealed that the residual stresses in diamond found after brazing are rather low (approximately between −325 MPa and −400 MPa) and exhibit only a slight dependence on the brazing parameters. At lower brazing temperatures a ductile fracture in the filler alloy is favoured, whereas at higher brazing temperatures it seems that the fracture is shifted into the brittle interlayers. It is concluded that the residual stresses are rather independent of the brazing parameters, whereas they strongly affect the microstructure and therefore the shear strengths of the joints. For this reason it is assumed that the best joint properties, i.e. low residual stresses and high shear strength, are obtained by brazing at the lowest temperature.

Acknowledgements The authors would like to thank the Swiss National Science Foundation for the financial support under the number 200021-117847. S.B. is grateful to Dr. H.-R. Elsener (Laboratory for Joining and Interface Technology, Empa, Duebendorf) for his support in brazing and Dr. T. Wermelinger (Laboratory for Nanometallurgy, ETH, Zurich) for fruitful discussions about Raman spectroscopy.

References

1. Burkhard G, Rehsteiner F (2002) CIRP Ann Manuf Technol 51:271
2. Fu YC, Xiao B, Xu JH, Xu HJ (2004) Key Eng Mater 259-2:73
3. Sung CM (1999) Diamond Relat Mater 8:1540
4. Sung JC, Sung M (2009) Int J Refract Met Hard Mater 27:382
5. Klotz UE, Liu CL, Khalid FA, Elsener HR (2008) Mater Sci Eng A 495:265
6. Liu CL (2007) Characterisation and modelling of interface reactions between diamond and active brazing alloys. Diss. ETH No. 17469, ETH Zurich, Switzerland
7. Paiva OC, Barbosa MA (2008) Mater Sci Eng A 480:306
8. De Wolf I (2003) Spectrosc Eur 15:6
9. Knight DS, White WB (1989) J Mater Res 4:385
10. Olson JM, Dawes MJ (1996) J Mater Res 11:1765
11. Aleksandrov IV, Goncharov AF, Stishov SM (1986) JETP Lett 44:611
12. Aleksandrov IV, Goncharov AP, Makarenko IN, Zisman AN, Jakovenko EV, Stishov SM (1989) High Press Res 1:333
13. Boppart H, Van Straaten J, Silvera IF (1985) Phys Rev B 32:1423
14. Grimsditch MH, Anastassakis E, Cardona M (1978) Phys Rev B 18:901
15. Hanfland M, Syassen K, Fahy S, Louie SG, Cohen ML (1985) Phys Rev B 31:6896
16. Mitra SS, Brafman O, Daniels WB, Crawford RK (1969) Phys Rev 186:942
17. Tardieu A, Cansell F, Petitet JP (1990) J Appl Phys 68:3243

18. Whalley E, Lavergne A, Wong PTT (1976) Rev Sci Instrum 47:845
19. Occelli F, Loubeyre P, Letoullec R (2003) Nat Mater 2:151
20. Kunc K, Loa I, Syassen K (2003) Phys Rev B 68:094107
21. Nielsen OH (1986) Physica B 139 & 140:202
22. Nielsen OH (1986) Phys Rev B 34:5808
23. Klocke F, Merbecks T (2001) Characterization of vitrified cBN grinding wheels. 4th int mach grind conf, Society of Manufacturing Engineers, Michigan
24. Dos Santos SI, Balzaretti NM, Da Jornada JAH (2006) Diamond Relat Mater 15:1457
25. Siegmann S, Dvorak M, Gruetzner H, Nassenstein K, Walter A (2005) Proc Int Therm Spray Conf 2005:823
26. Mizuhara H, Huebel E, Oyama T (1989) Am Ceram Soc Bull 68:1591
27. ElementSix-website (2009) Isle of Man, United Kingdom. http://www.e6.com. Accessed 9 Oct 2009
28. Wegst C, Wegst M (2007) Nachschlagewerk Stahlschüssel. Verlag Stahlschüssel Wegst GmbH, Marbach
29. Field JE (1979) The properties of diamond. Academic Press, London
30. Ikawa N, Shimada S, Ono T (1976) Technol Rep Osaka Univ 26:245
31. Ganesan S, Maradudin AA, Oitmaa J (1970) Ann Phys 56:556
32. Anastassakis E, Pinczuk A, Burstein E, Pollak FH, Cardona M (1970) Solid State Commun 8:133
33. Englert T, Abstreiter G, Pontcharra J (1980) Solid-State Electron 23:31
34. Klocek P (1991) Handbook of infrared optical materials. Marcel Dekker, Inc., New York
35. Cousins CSG (2003) Phys Rev B 67:024107-1-13
36. Chen KH, Lai YL, Lin JC, Song KJ, Chen LC, Huang CY (1995) Diamond Relat Mater 4:460
37. Loechelt GH, Cave NG, Menendez J (1999) J Appl Phys 86:6164
38. Feng JC, Li YL, He P, Liu HJ, Yan JC (2005) Mater Sci Technol 21:255
39. Kar A, Ghosh M, Ray AK, Ray AK (2008) Mater Sci Eng A 498:283
40. Duhaj P, Sebo P, Svec P, Janickovic D (1999) Mater Sci Eng A 271:181
41. Groegler T, Zeiler E, Hoerner A, Rosiwal SM, Singer RF (1998) Surf Coat Technol 98:1079
42. Scardi P, Leoni M, Cappuccio G, Sessa V, Terranova ML (1997) Diamond Relat Mater 6:807
43. Fu YQ, Du HJ, Sun CQ (2003) Thin Solid Films 424:107
44. Fan QH, Gracio J, Pereira E, Teixeira V, Tavares CJ (2001) Thin Solid Films 398:265
45. Ralchenko VG, Obraztsova ED, Korotushenko KG, Smolin AA, Pimenov SM, Pereverzev VG (1995) Mechanical behaviour of diamond and other forms of carbon, Mater Res Soc Symp Proc, Materials Research Society, Pittsburgh, PA ,vol 383, pp 153–158
46. Kohzaki M, Higuchi K, Noda S, Uchida K (1993) Diamond Relat Mater 2:612
47. Qin YQ, Feng JC (2007) Mater Sci Eng A 454:322
48. Sun FL, Feng JC, Li D (2001) J Mater Process Technol 115:333